



## Article

# Inhibiting AGS Cancer Cell Proliferation through the Combined Application of Aucklandiae Radix and Hyperthermia: Investigating the Roles of Heat Shock Proteins and Reactive Oxygen Species

Chae Ryeong Ahn <sup>1</sup>, In Jin Ha <sup>2</sup>, Jai-Eun Kim <sup>1</sup>, Kwang Seok Ahn <sup>3</sup>, Jinbong Park <sup>3,\*</sup>  
and Seung Ho Baek <sup>1,\*</sup>

- <sup>1</sup> College of Korean Medicine, Dongguk University, 32 Dongguk-ro, Ilsandong-gu, Goyang-si 10326, Republic of Korea  
<sup>2</sup> Korean Medicine Clinical Trial Center (K-CTC), Korean Medicine Hospital, Kyung Hee University, Seoul 02447, Republic of Korea  
<sup>3</sup> College of Korean Medicine, Kyung Hee University, 24 Kyungheedaero, Dongdaemun-gu, Seoul 02447, Republic of Korea  
\* Correspondence: thejin bong@khu.ac.kr (J.P.); baekone99@gmail.com (S.H.B.)

**Abstract:** Cancer is a major global health concern. To address this, the combination of traditional medicine and newly appreciated therapeutic modalities has been gaining considerable attention. This study explores the combined effects of Aucklandiae Radix (AR) and 43 °C hyperthermia (HT) on human gastric adenocarcinoma (AGS) cell proliferation and apoptosis. We investigated the synergistic effects of AR and HT on cell viability, apoptosis, cell cycle progression, and reactive oxygen species (ROS)-dependent mechanisms. Our findings suggest that the combined treatment led to a notable decrease in AGS cell viability and increased apoptosis. Furthermore, cell cycle arrest at the G2/M phase contributed to the inhibition of cancer cell proliferation. Notably, the roles of heat shock proteins (HSPs) were highlighted, particularly in the context of ROS regulation and the induction of apoptosis. Overexpression of HSPs was observed in cells subjected to HT, whereas their levels were markedly reduced following AR treatment. The suppression of HSPs and the subsequent increase in ROS levels appeared to contribute to the activation of apoptosis, suggesting a potential role for HSPs in the combined therapy's anti-cancer mechanisms. These findings provide valuable insights into the potential of integrating AR and HT in cancer and HSPs.

**Keywords:** Aucklandiae Radix; cancer; heat shock proteins; hyperthermia; reactive oxygen species



**Citation:** Ahn, C.R.; Ha, I.J.; Kim, J.-E.; Ahn, K.S.; Park, J.; Baek, S.H. Inhibiting AGS Cancer Cell Proliferation through the Combined Application of Aucklandiae Radix and Hyperthermia: Investigating the Roles of Heat Shock Proteins and Reactive Oxygen Species. *Antioxidants* **2024**, *13*, 564. <https://doi.org/10.3390/antiox13050564>

Academic Editor: David Arráez-Román

Received: 10 March 2024  
Revised: 25 April 2024  
Accepted: 29 April 2024  
Published: 3 May 2024



**Copyright:** © 2024 by the authors. Licensee MDPI, Basel, Switzerland. This article is an open access article distributed under the terms and conditions of the Creative Commons Attribution (CC BY) license (<https://creativecommons.org/licenses/by/4.0/>).

## 1. Introduction

Cancer remains a health challenge and is a leading cause of mortality worldwide, necessitating the development of effective and innovative treatment strategies [1–4]. Recently, the therapeutic paradigm has shifted towards a combination of different modalities to enhance treatment efficacy and potentially reduce associated side effects [5–8]. In particular, the integration of traditional herbal medicine with alternative therapeutic approaches such as hyperthermia (HT) has gained significant attention [9–11].

Aucklandiae Radix (AR), also known as Muxiang in traditional Chinese medicine, is a well-known medicinal herb with a rich history of therapeutic usage [12–15]. Extracted from the root of *Aucklandia lappa* DC., AR has been extensively used in various traditional medicinal systems for its broad-spectrum therapeutic properties [16–18]. Applications include the treatment of gastrointestinal disorders, alleviation of pain, and mitigation of inflammatory responses [19]. Among the diverse bioactive constituents of AR, costunolide and dehydrocostus lactone stand out for their potent anti-cancer activities [20–22]. Both compounds belong to the sesquiterpene lactone family; a class of compounds recognized

for their cytotoxic effects against a variety of cancer cells [23,24]. Previous studies have suggested that the anti-cancer effects of these compounds are primarily mediated by the induction of reactive oxygen species (ROS).

ROS includes free radicals such as superoxide and hydroxyl radicals, and non-radicals such as hydrogen peroxide. ROS plays dual roles in cancer biology [25]. Under physiological conditions, ROS contribute to cellular homeostasis by modulating cellular signaling pathways [26]. However, when overproduced or insufficiently neutralized, ROS can induce oxidative stress, leading to cellular damage, apoptosis, and autophagy, making ROS generation a common target for anti-cancer strategies [27]. Costunolide and dehydrocostus lactone have been found to provoke a surge in ROS within cancer cells, thus tipping the balance towards apoptosis, the programmed cell death process that is often dysfunctional in cancer cells [28]. By triggering ROS-induced apoptosis, these compounds can effectively counteract the unchecked proliferation of cancer cells, which is a hallmark of cancer.

HT, the targeted application of heat to the body tissues, is emerging as an effective adjuvant therapy for cancer treatment [29–31]. Increasing the temperature of cancer cells increases their susceptibility to other anti-cancer therapies [32]. Mild HT, specifically around 43 °C, has shown promising results in combination with other treatments.

Heat shock proteins (HSPs) are intracellular proteins whose expression increases in response to stresses such as heat [33]. In the context of cancer, HSPs play critical roles in cell survival, proliferation, and therapeutic resistance [34,35]. They also help in maintaining intracellular homeostasis by preventing the accumulation of harmful ROS [36]. However, overexpression of HSPs in cancer cells aids their survival, thus contributing to disease progression.

Despite the established individual effectiveness of AR and HT and the known role of HSPs in cancer, the collective impact of these factors, particularly on human gastric adenocarcinoma (AGS) cells, is not well understood. Understanding the mechanisms underlying the potential synergistic effects of AR, HT, and HSPs could provide valuable insights into more effective cancer treatments. In this study, we explore the combined effects of AR and 43 °C HT on AGS cancer cell proliferation, apoptosis, and the role of HSPs and ROS in these processes. Based on the bioactive properties of costunolide and dehydrocostus lactone and their roles in ROS generation, we hypothesized that these compounds could significantly contribute to the observed therapeutic effects of the combined treatment. We also investigated the role of HSPs in this context, particularly in response to co-treatment with AR and HT. These findings could help pave the way for future research on the potential benefits of combined herbal and HT therapies in cancer treatment, considering the role of HSPs and ROS.

## 2. Materials and Methods

### 2.1. Preparation of AR Extract

AR (Kwangmyeongdang Medicinal Herbs Co. Ltd., Ulsan, Republic of Korea) was ground, extracted for 24 h at room temperature with 1 L of 70% EtOH, and filtered (pore size: 5 µm) using vacuum concentration and lyophilization. Prior to use, the drugs were kept at 4 °C, and dimethyl sulfoxide (DMSO) (Samcheon Chemical, Seoul, Republic of Korea) was used to produce concentrations of 10, 15, and 20 µg/mL.

### 2.2. Liquid Chromatography (LC)–Mass Spectrometry (MS) Analysis

Chemical components of AR were analyzed using ultra-performance liquid chromatography–electrospray ionization/quadrupole time-of-flight high-definition mass spectrometry (UPLC-ESI-QTOF-MS/MS). To prepare the sample, the extract was agitated for 30 s in 50% methanol using a vortex mixer, followed by 10 min of sonication. Subsequently, the supernatants were filtered through a 0.2 µm hydrophilic polytetrafluoroethylene syringe filter (Thermo Fisher Scientific, Sunnyvale, CA, USA). The filtered extract was then diluted to 100 mg/mL and transferred to an LC vial for analysis. The analysis was conducted using a Thermo Scientific Vanquish UHPLC system coupled with a Poeshell EC-C18 column (2.1 mm × 100 mm,

2.7  $\mu\text{m}$ ; Agilent, Santa Clara, CA, USA) and a Triple TOF5600+ mass spectrometer system (QTOF MS/MS, SCIEX, Foster City, CA, USA).

The QTOF MS system featured an electrospray ionization (ESI) source operable in both positive and negative ion modes for high-resolution experiments. The elution program for UHPLC involved 0.1% formic acid in water as eluent A and methanol as eluent B, progressing as follows: 0–10 min at 5% B; 10–30 min ramping from 5% to 80% B; 30–31 min from 80% to 100% B; 31–35 min at 100% B; and a 4 min equilibration at 5% B, with a flow rate of 0.3 mL/min. The column temperature was set at 25 °C and the autosampler temperature at 4 °C. Each sample was injected in a volume of 5  $\mu\text{L}$ . Data for qualitative analysis were acquired and processed using Analyst TF 1.7, PeakView 2.2, and MasterView software 4.5 (SCIEX, Foster City, CA, USA), with MS/MS data further analyzed in PeakView and MasterView to identify probable metabolites based on accurate mass and isotopic distributions.

### 2.3. Cell Culture

AGS stomach cancer cells were obtained from the Korean Cell Line Bank (Seoul, Republic of Korea). The cells were maintained in an incubator at 37 °C with humidified air containing 5%  $\text{CO}_2$ , in Dulbecco's modified eagle medium (DMEM) supplemented with 10% fetal bovine serum (FBS; heat-inactivated) (Gibco, Grand Island, NY, USA) and 1% of Pen-Strep (10,000 U/mL) (Gibco, Grand Island, NY, USA).

### 2.4. HT Treatment

AR was applied to the samples at the designated concentrations, and after an hour, AGS cells ( $0.3 \times 10^6$  cells/well) were seeded and suspended in 3 mL of media before being incubated in a water bath at 37 or 43 °C for 30 min.

### 2.5. MTT Assay

The 3-(4,5-dimethylthiazol-2-yl)-2,5-diphenyltetrazolium bromide (MTT) assay was used to confirm the synergistic effect of concurrent drug and heat treatment. AGS cells ( $1 \times 10^4$  cells/mL) were plated on a 6-well plate, treated with 0, 10, 15, and 20  $\mu\text{g}/\text{mL}$  of AR for an hour, and then exposed to 37 or 43 °C for 30 min. Twenty microliters per well of MTT reagent (2 mg/mL in phosphate-buffered saline; PBS) (AMRESCO, Solon, OH, USA) were added after 48 h of incubation. The wells were then incubated at 37 °C for 2 h in the dark. Following suction, 100  $\mu\text{L}$  of DMSO was added to each well, the mixture was agitated, and the absorbance at 570 nm was determined using a spectrophotometric plate reader. Relative cell viability was standardized against untreated controls.

### 2.6. Trypan Blue Assay

Cell viability was determined using a trypan blue (Sigma-Aldrich, St. Louis, MO, USA) assay. After seeding, AGS cells ( $0.3 \times 10^6$  cells/mL) were treated with AR at 20  $\mu\text{g}/\text{mL}$  (control: 0  $\mu\text{g}/\text{mL}$  AR) and allowed to react for 1 h, after which they were exposed to 37 or 43 °C for 30 min. After 24 h, the cells were collected, stained with a 1:4 diluted solution of 1  $\times$  PBS and trypan blue reagent, and counted using a hemocytometer. Cell survival was determined by

$$\text{cell survival (\%)} = \frac{\text{viable cell count}}{\text{total cell count}} \times 100$$

### 2.7. Morphology Assay

A morphology assay was performed to assess cell proliferation. AGS cells were seeded in a 6-well plate ( $0.3 \times 10^6$  cells per well). After adherence, the cells were treated with 20  $\mu\text{g}/\text{mL}$  AR for 1 h, and then incubated at 37 or 43 °C for an additional 30 min. Twenty-four hours later, cells were analyzed and imaged using an Olympus CX-40 microscope (Olympus, Tokyo, Japan).

### 2.8. Wound Healing Assay

AGS cells were seeded in a 6-well plate ( $0.3 \times 10^6$  cells/well) and then cultured at  $37^\circ\text{C}$  in an incubator. A thin scratch was made in each well with a micropipette tip, and the wells were treated with AR (20  $\mu\text{g}/\text{mL}$ ) and HT. Images were obtained using an Olympus CX-40 microscope (Olympus, Tokyo, Japan) at 0 and 24 h

### 2.9. Colony Formation Assay

Each well of a 6-well plate was filled with 400 cells, and the plates were incubated overnight. The cells were treated with 20  $\mu\text{g}/\text{mL}$  AR for an hour after a 30 min incubation period at  $37$  or  $43^\circ\text{C}$ . After two weeks, the cells were washed with  $1 \times$  PBS and stained with a crystal violet solution (Sigma-Aldrich, St. Louis, MO, USA) for 10 min at room temperature. An Olympus CX-40 microscope (Olympus, Tokyo, Japan) was used to examine the colonies.

### 2.10. Western Blot Analysis

Western blot analysis was performed as previously described [9]. Primary antibodies of anti-caspase-3, anti-caspase-8, anti-caspase-9, anti-p-ERK (Thr202/Tyr204), anti-ERK, anti-p-JNK (Thr183/Tyr185), anti-JNK, anti-p-p38 (Thr180/Tyr182), anti-p38, anti-HSP27, anti-HSP70, anti-HSP90 (Cell Signaling Technology, Danvers, MA, USA), anti- $\beta$ -actin, anti-Bcl-2, anti-Bcl-xL, anti-Cyclin B1, anti-Cyclin D1, anti-MMP2, anti-MMP9, anti-VEGF (Santa Cruz Biotechnology, Inc., Dallas, TX, USA), and anti-cleaved caspase-3 (GeneTex) were used. Membranes were visualized using enhanced chemiluminescence (ECL) (Millipore, Billerica, MA, USA).

### 2.11. Apoptosis Assay

The apoptosis assay was performed using an Annexin V-fluorescein isothiocyanate (FITC) Detection Kit (ApoScan kit, Cat. No.: LS-02-100). AGS cells ( $0.3 \times 10^6$  cells/well in a 6-well plate) were treated with 0 and 20  $\mu\text{g}/\text{mL}$  concentrations of AR for 1 h, followed by exposure to temperatures of  $37^\circ\text{C}$  or  $43^\circ\text{C}$  for 30 min. After 24 h, the cells were harvested and stained with Annexin V-FITC for 15 min at room temperature in the dark, as per the manufacturer's instructions. Subsequent to staining, the cells underwent centrifugation to discard the supernatant, and propidium iodide (PI) staining was applied using  $1 \times$  cold binding buffer. Apoptosis levels were quantified via flow cytometry.

### 2.12. Cell Cycle Analysis

AGS cells ( $0.3 \times 10^6$  cells/well in 6-well plates) treated simultaneously with AR and HT for 24 h for cell cycle analysis. Then, the cells were collected, fixed in 70% ethanol for 24 h, and subsequently washed with  $1 \times$  cold PBS. The cells were then resuspended in PBS containing 1 mg/mL PI and 10 mg/mL RNase A, and incubated in the dark for 10 min. Cell cycles were assessed using a flow cytometer.

### 2.13. Analysis of ROS

H2DCFDA (2',7'-dichlorofluorescein diacetate or Invitrogen™ D399; Thermo Fisher Scientific) reagent was used to measure cellular ROS. After seeding the AGS cells ( $0.3 \times 10^6$  cells/well), they were co-treated and then incubated. After 4 h, the cells were harvested to obtain a pellet, and 10  $\mu\text{M}$  H2DCFDA reagent was added, followed by a 40 min incubation at  $37^\circ\text{C}$  in the dark. Flow cytometry was used to calculate ROS levels.

### 2.14. Statistical Analysis

The mean  $\pm$  SD is used to represent all numerical values. Statistical significance was determined using Student's unpaired *t*-tests. \*  $p < 0.05$ , \*\*  $p < 0.01$  and \*\*\*  $p < 0.001$ .

### 3. Results

#### 3.1. Chemical Components of AR Identified by UPLC-ESI-QTOF-MS/MS

The ethanolic extract was analyzed by UPLC-ESI-QTOF-MS/MS analysis to determine the chemical profile of its constituents. The extracted ion chromatogram identified 14 components including costunolide (**13**) and dehydrocostus lactone (**14**), which are the two main compounds in AR (Figure 1). Area under curve shows that costunolide (**13**) accounts for 9.74% and dehydrocostus lactone (**14**) accounts for 10.02%. Of note, 3,4-dicaffeoylquinic acid (**7**) accounted for 0.40%, parthenolide (**11**) for 0.36%, tryptophan (**2**) for 0.07%, syringaldehyde (**5**) for 0.03%. Detailed information of the detected peaks is listed in Table 1.

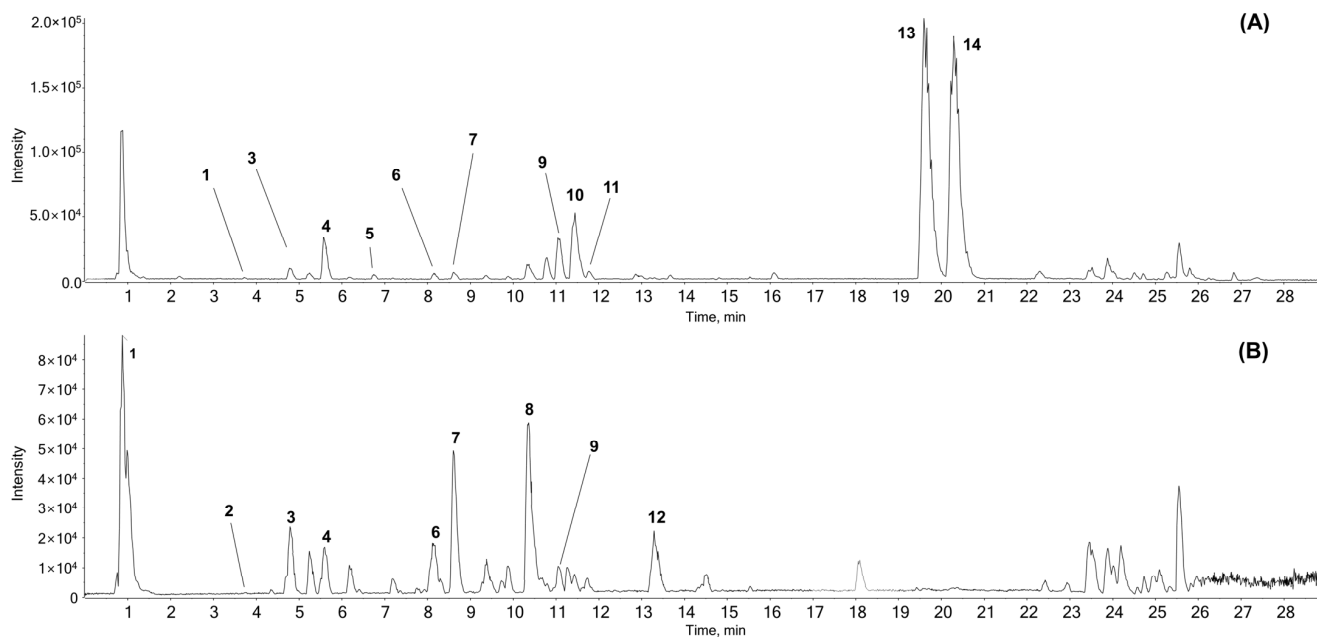


**Figure 1.** Representative base peak chromatogram of AR using UPLC-ESI-QTOF MS/MS analysis in (A) positive and (B) negative ion modes. AR, Aucklandiae Radix; UPLC-ESI-QTOF MS/MS, ultra-performance liquid chromatography-electrospray ionization/quadrupole time-of-flight mass spectrometry/mass spectrometry.

**Table 1.** Detected peak list from the UPLC-ESI-QTOF-MS/MS analysis of AR.

No.	Name	Formula	Mass (Da)	Expected RT (min)	Adduct	Found at Mass (Da)	Error (ppm)	MS/MS Product ions	Identified with
1	Citric acid	C <sub>6</sub> H <sub>8</sub> O <sub>7</sub>	192.027	1.05	[M – H] <sup>–</sup>	191.0199	0.9	111.0101, 87.01303, 85.0309	#
2	Tryptophan	C <sub>11</sub> H <sub>12</sub> N <sub>2</sub> O <sub>2</sub>	204.08988	3.73	[M + H] <sup>+</sup>	205.09696	–1	188.0686, 143.0728, 144.0801	#
					[M – H] <sup>–</sup>	203.08269	0.5	116.0497, 142.0670, 74.0270	
3	Chlorogenic acid	C <sub>16</sub> H <sub>18</sub> O <sub>9</sub>	354.09508	4.72	[M + H] <sup>+</sup>	355.1026	0.7	163.0384, 145.0276, 135.0435, 117.0332	#
					[M – H] <sup>–</sup>	353.08777	–0.1	191.0557, 161.0237, 173.0439	
4	Unknown	C <sub>26</sub> H <sub>39</sub> NO <sub>10</sub>	525.2574	5.6	[M + H] <sup>+</sup>	526.26426	–0.8	364.2122, 128.0708, 346.2013	*
					[M – H] <sup>–</sup>	524.24949	–1.2	114.0566, 209.1889, 247.1327	
5	Syringaldehyde	C <sub>9</sub> H <sub>10</sub> O <sub>4</sub>	182.05791	6.83	[M + H] <sup>+</sup>	183.0651	–0.6	77.0402, 95.0497, 140.0465, 123.0442	#

Table 1. Cont.

No.	Name	Formula	Mass (Da)	Expected RT (min)	Adduct	Found at Mass (Da)	Error (ppm)	MS/MS Product ions	Identified with
6	1,5-Dicaffeoylquinic acid	C <sub>25</sub> H <sub>24</sub> O <sub>12</sub>	516.12678	8.15	[M + H] <sup>+</sup>	517.13348	−1.1	163.0386, 145.0280, 135.0445, 319.0813	#
					[M − H] <sup>−</sup>	515.11915	−0.7	191.0558, 353.0873, 179.0341, 161.0245	
7	3,4-Dicaffeoylquinic acid	C <sub>25</sub> H <sub>24</sub> O <sub>12</sub>	516.12678	8.63	[M + H] <sup>+</sup>	517.13357	−0.9	163.0384, 145.0289, 135.0445, 319.0809	#
					[M − H] <sup>−</sup>	515.11901	−0.9	353.0876, 173.0451, 179.0346, 191.0551	
8	Unknown	C <sub>22</sub> H <sub>32</sub> O <sub>10</sub>	456.19955	10.35	[M − H] <sup>−</sup>	455.1917	−1.2	247.1333, 409.1877, 203.1431, 135.0809	*
9	Unknown	C <sub>20</sub> H <sub>27</sub> NO <sub>4</sub>	345.19401	11.07	[M + H] <sup>+</sup>	346.20148	0.5	100.0766, 88.0668, 70.0671	+
					[M − H] <sup>−</sup>	344.18673	0	114.0572, 113.0690	
10	Unknown	C <sub>21</sub> H <sub>28</sub> N <sub>2</sub> O	324.22016	11.43	[M + H] <sup>+</sup>	325.22767	0.7	91.0560, 86.0983, 233.1653, 84.0825	*
11	Parthenolide	C <sub>15</sub> H <sub>20</sub> O <sub>3</sub>	248.14124	11.77	[M + H] <sup>+</sup>	249.14857	0.6	185.1325, 143.0856, 128.0617, 129.0696	#
12	Unknown	C <sub>18</sub> H <sub>34</sub> O <sub>5</sub>	330.24062	13.33	[M − H] <sup>−</sup>	329.23305	−0.9	211.1342, 229.1444, 171.1028, 139.1135	*
								187.1482, 145.1017, 131.0854, 105.0708, 91.0554	
13	Costunolide <sup>†</sup>	C <sub>15</sub> H <sub>20</sub> O <sub>2</sub>	232.14633	19.63	[M + H] <sup>+</sup>	233.15364	0.2	143.0861, 128.0624, 129.0705, 185.1332	*
14	Dehydrocostuslactone <sup>†</sup>	C <sub>15</sub> H <sub>18</sub> O <sub>2</sub>	230.13068	20.30	[M + H] <sup>+</sup>	231.13814	0.8		#

# In-house ms/ms library and online database; such as GNPS, MASS bank or Metlin. † Reference standard, \* Extract MS with isotope mass.

### 3.2. Co-Treatment with AR and 43 °C HT Synergistically Inhibited AGS Cell Proliferation

The combination of AR and 43 °C exhibited a synergistic effect in hampering the proliferation of AGS cells. To test the efficacy of the treatments, we conducted MTT assays. When subjected to an identical dose of AR (20 µg/mL), we observed that AGS cell viability was reduced more notably by the combined treatment with 43 °C HT than the one with 37 °C (Figure 2A). This effect of the combination of AR and HT was further substantiated by trypan blue staining of surviving cells (Figure 2B) and an apparent alteration in cell morphology (Figure 2C). Upon evaluation of crystal violet-stained AGS cells, the combination treatment with AR and 43 °C resulted in a significant drop in colony formation relative to the treatment involving AR and 37 °C (Figure 2D). The subsequent cell migration analysis revealed that the combination of AR and HT inhibited cell migration (Figure 2E).

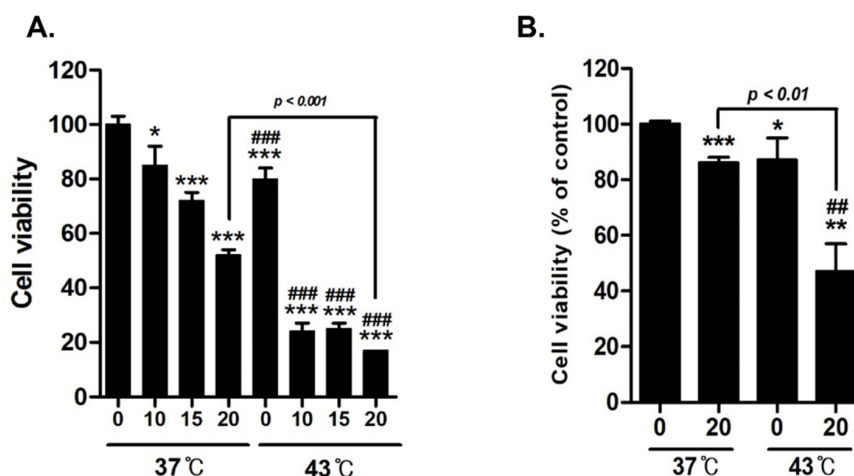
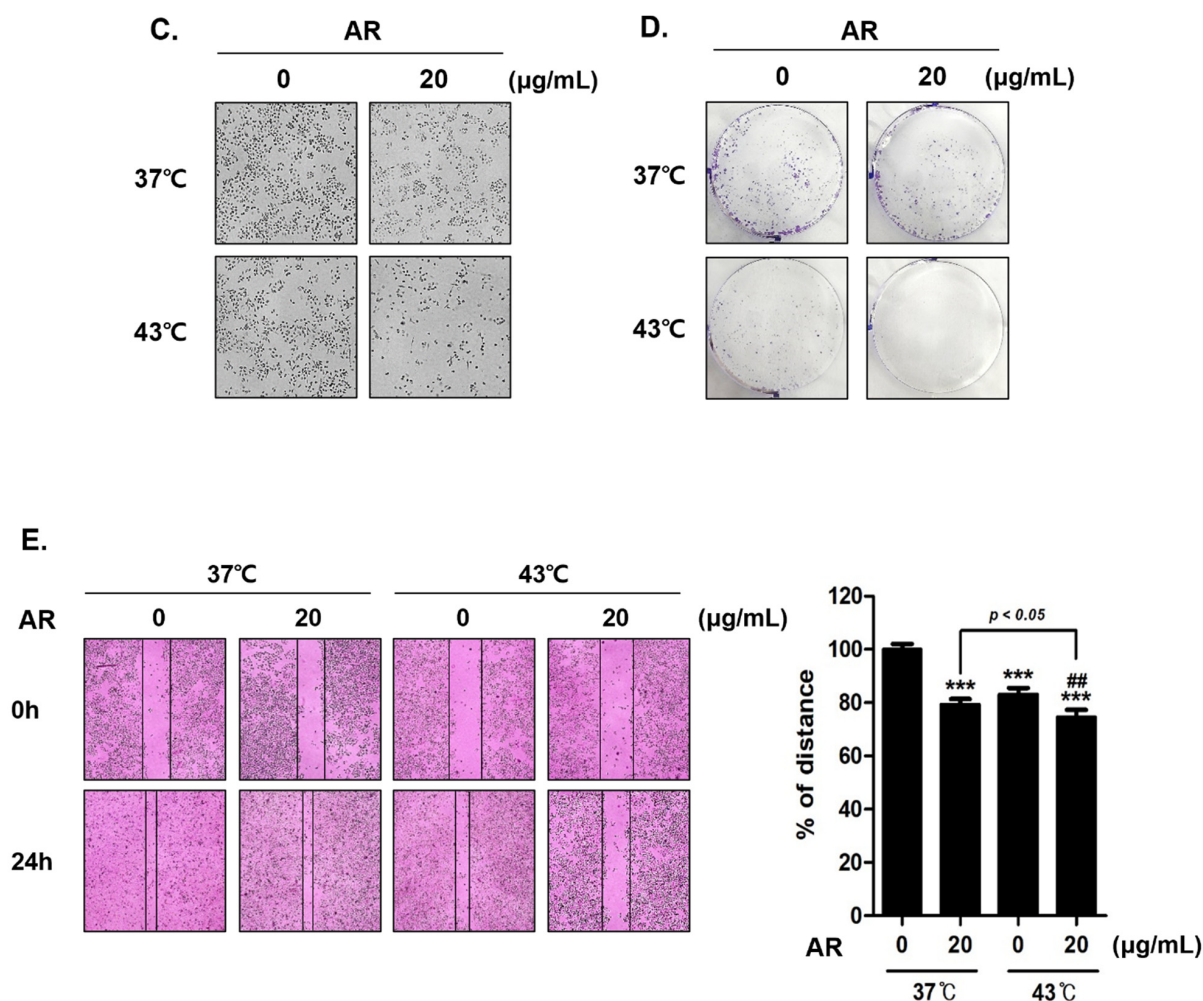


Figure 2. Cont.



**Figure 2.** Effect of AR and HT on AGS cell viability. AGS cells were treated with various concentrations of AR (0, 10, 15, and 20 µg/mL) for 24 h with (at 43 °C) or without (at 37 °C) HT. (A) Percentage cell viability was determined using the MTT assay. (B) The trypan blue staining was performed to determine live cell percentage under a regular light microscope. (C) Apoptosis-related morphological changes as seen at 100× magnification. (D) For the clonogenic experiment, crystal violet staining was utilized. (E) Wound healing assays were performed to determine changes in cell migration of control and treated cells at 0 and 24 h. Bar graphs indicate the gap distance percentage at hour 24 compared to hour 0. \*  $p < 0.05$ , \*\*  $p < 0.01$ , \*\*\*  $p < 0.001$  vs. control group; ##  $p < 0.01$ , ###  $p < 0.001$  vs. 43 °C + 0 µg/mL group.

### 3.3. The Combined Application of AR and 43 °C HT Enhanced the Manifestation of Factors Associated with Apoptosis and Suppressed Factors Related to Protection and Proliferation in AGS Cells

In the next phase of our research, we validated the expression levels of factors associated with processes such as apoptosis, cell proliferation, metastasis/angiogenesis to elucidate the synergistic mechanism triggered by concurrent treatment with AR and HT. As depicted in Figure 3A, a combined treatment with AR and HT at 43 °C significantly promoted the cleavage of caspase-3, which signifies the culmination of programmed apoptosis [37]. This phenomenon was not evident when AR was paired with an HT of 37 °C. We assessed caspase-8 and caspase-9, which are the primary caspases associated with extrinsic and intrinsic apoptosis, respectively (Figure 3B) [38]. In accordance with the findings related to cleaved caspase-3, caspase-8 and -9 expression decreased in a dose-dependent manner, but only when subjected to a combined treatment with AR and 43 °C HT. Furthermore, concurrently treating with AR and 43 °C HT led to a dose-dependent

decrease in the expression levels of anti-apoptotic constituents of the B-cell lymphoma (Bcl)-2 family, which included Bcl-2 and Bcl-xL (Bcl-extra large) (Figure 3C) [39]. Our study also examined Cyclin D1 [40], a modulator of cell adhesion and migration linked to cancer cell invasion and metastasis; vascular endothelial growth factor (VEGF) [41], a central molecule in angiogenesis; and matrix metalloproteinase (MMP)-9, an instrumental member of the MMP family implicated in tumor metastasis [42]. Our data unequivocally demonstrated that these metastatic factors were curtailed by the combination of AR and 43 °C HT (Figure 3D).

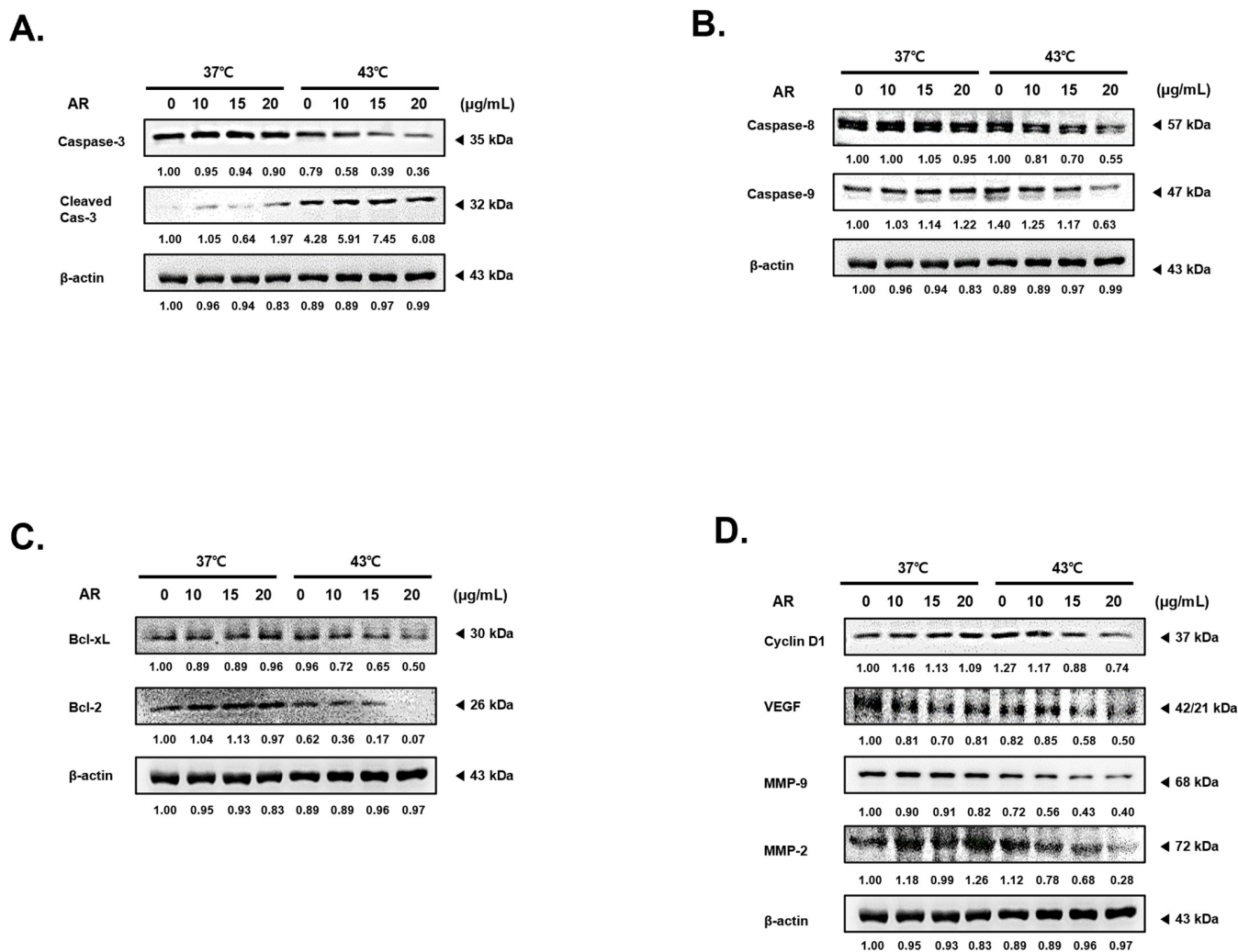


**Figure 3.** Effect of AR and HT on survival, proliferation, and angiogenesis expression levels in the treatment and control groups. The protein expressions of (A) caspase-3, (B) caspase-8, caspase-9, (C) Bcl-xL, Bcl-2, and (D) Cyclin D1, VEGF, MMP-9, and MMP-2 were determined by Western blot. β-actin was used as a loading control. Bcl, B-cell lymphoma; xL, extra large; VEGF, vascular endothelial growth factor; MMP, matrix metalloproteinase.

*3.4. The Combined Application of AR and 43 °C HT Induced Apoptosis and Cell Cycle Arrest in AGS Cells*

As demonstrated in Figure 4A, the combined treatment with AR and 43 °C HT increased apoptosis linked to Annexin V in AGS cells, and notably more than the 43 °C HT on its own or AR paired with normothermia. The cooperative influence of AR and HT was dose-dependent; the proportion of apoptotic cells increased from 2.85% (0 µg/mL AR, 37 °C) through 8.77% (20 µg/mL AR, 37 °C) and 12.59% (0 µg/mL AR, 43 °C) to 28.05% (20 µg/mL AR, 43 °C).

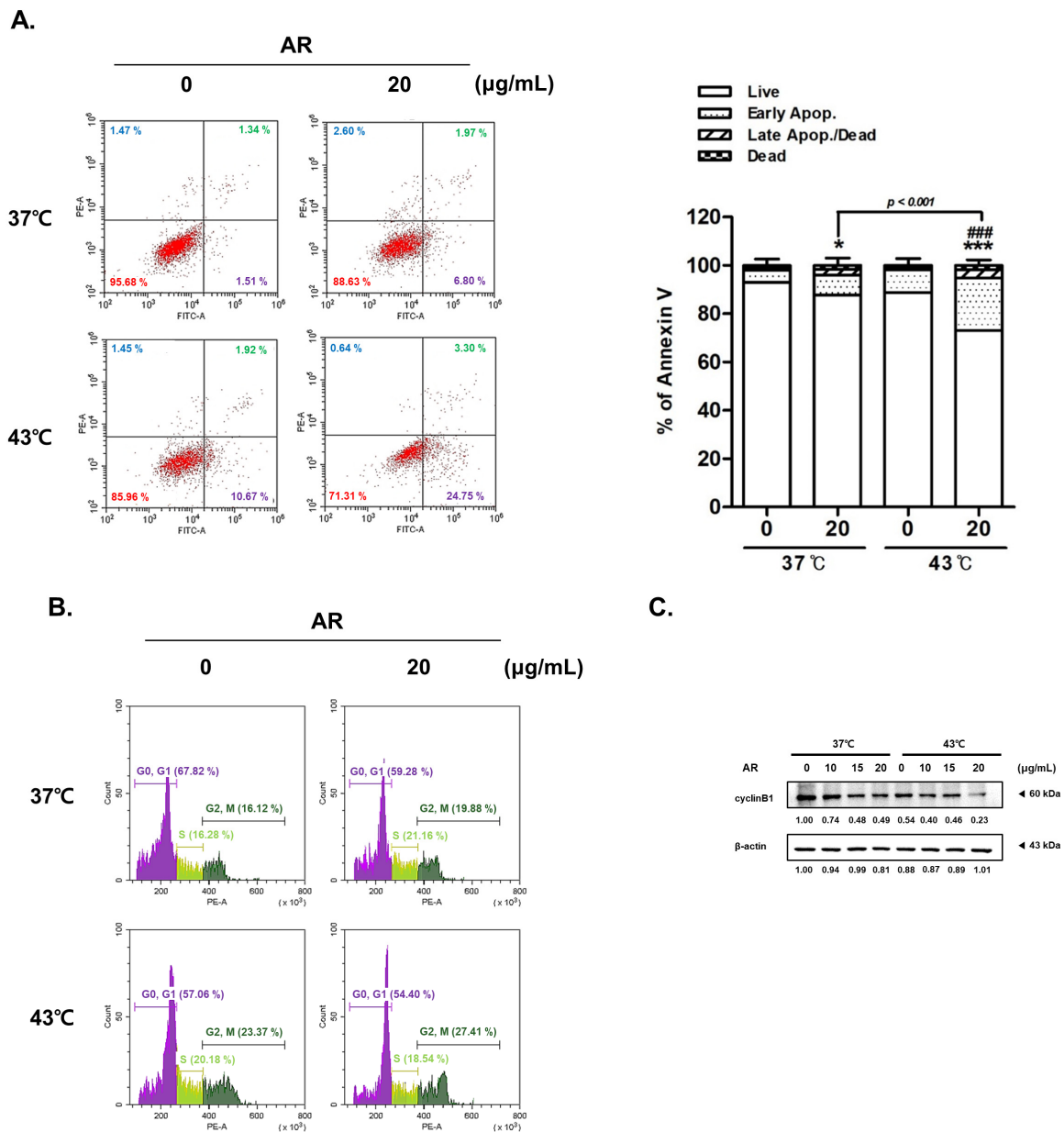


**Figure 4.** Effect of AR and HT on the cell cycle and apoptosis in AGS cells. AR (0 or 20 µg/mL) was applied to AGS cells ( $0.3 \times 10^6$  cells) with or without HT. Flow cytometry was used to determine apoptosis with Annexin V and PI staining. (A) Apoptosis profile and (B) cell cycle profile. (C) A Western blot assay was used to gauge Cyclin B1 expression. A loading control was performed with β-actin. Apop., apoptosis. \*  $p < 0.05$ , \*\*\*  $p < 0.001$  vs. control group; ###  $p < 0.001$  vs. 43 °C + 0 µg/mL group.

Cell cycle arrest is closely associated with the induction of apoptosis [43]. This process is a common therapeutic target for cancer treatment [44]. Flow cytometry was performed to establish whether the combined treatment with AR and HT had any effect on cell cycle arrest. We found that the combined treatment with AR and 43 °C HT halted the cell cycle in the gap 2/mitosis (G2/M) phase (Figure 4B) [45]. The treatment with AR in conjunction with 43 °C HT also significantly diminished cyclin B1 expression, thereby supporting the hypothesis that the co-treatment of AR and HT induces cell cycle arrest in AGS cells during the G2/M phase (Figure 4C). Taken together, these findings provide compelling evidence of the potential benefits of combining AR with 43 °C HT in inducing apoptosis and arresting the cell cycle in AGS cells, thereby providing novel insights into promising therapeutic approaches for cancer treatment.

3.5. The Combined Application of AR and 43 °C HT Synergistically Inhibited HSP Expression, Leading to ROS-Dependent Apoptosis

HSPs are known for their role in eliminating appropriate amounts of ROS from cancer cells, thereby facilitating their growth [46]. Therefore, we investigated how the combined application of AR and 43 °C HT could influence HSP expression and ROS levels. As in Figure 5A, HSPs 27, 70, and 90 were increased in AGS cells upon incubation at 43 °C HT, as expected. Treatment with AR markedly decreased HSP expression under HT. Considering the decreased expression of HSPs, co-treatment can augment ROS levels, which can activate mitogen-activated protein kinases (MAPKs), leading to the consequent induction of apoptosis [47]. As shown in Figure 5B, co-treatment boosted the phosphorylation of MAPKs, including Jun N-terminal kinase (JNK), p38, and extracellular signal-regulated kinase (ERK), at 43 °C HT. We also observed that co-treatment increased ROS production and decreased ROS levels following N-acetyl-L-cysteine (NAC) pretreatment. Subsequently, we conducted an experiment to establish the correlation between ROS production (Figure 5C) and the effectiveness of co-treatment. As shown in Figure 5D, the co-treatment demonstrated a synergistic effect, inducing apoptosis in cancer cells. However, NAC pretreatment mitigated this effect. Without the ROS signaling, combination treatment with AR and HT fail to interrupt the self-protection system induced by heat shock.

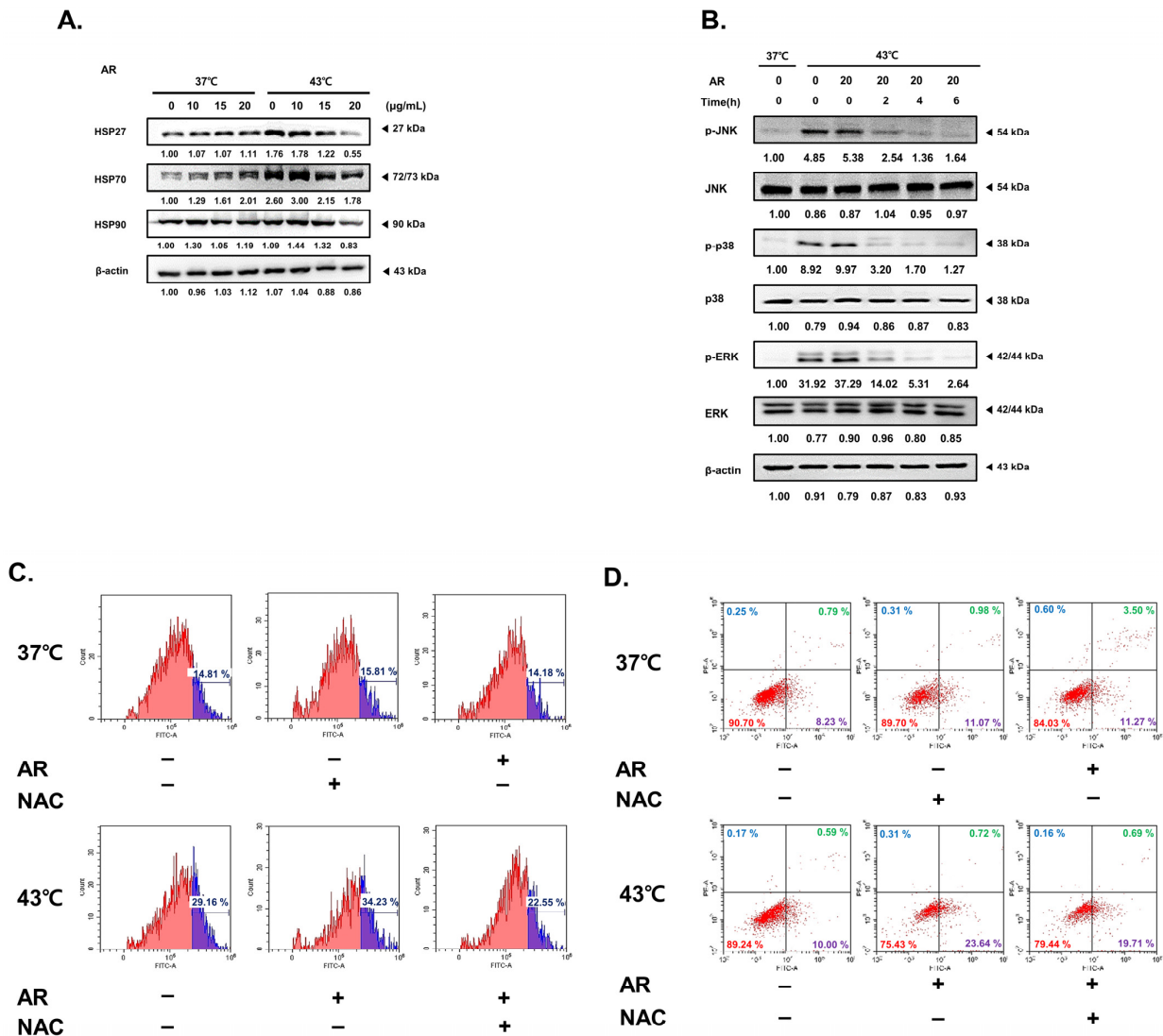
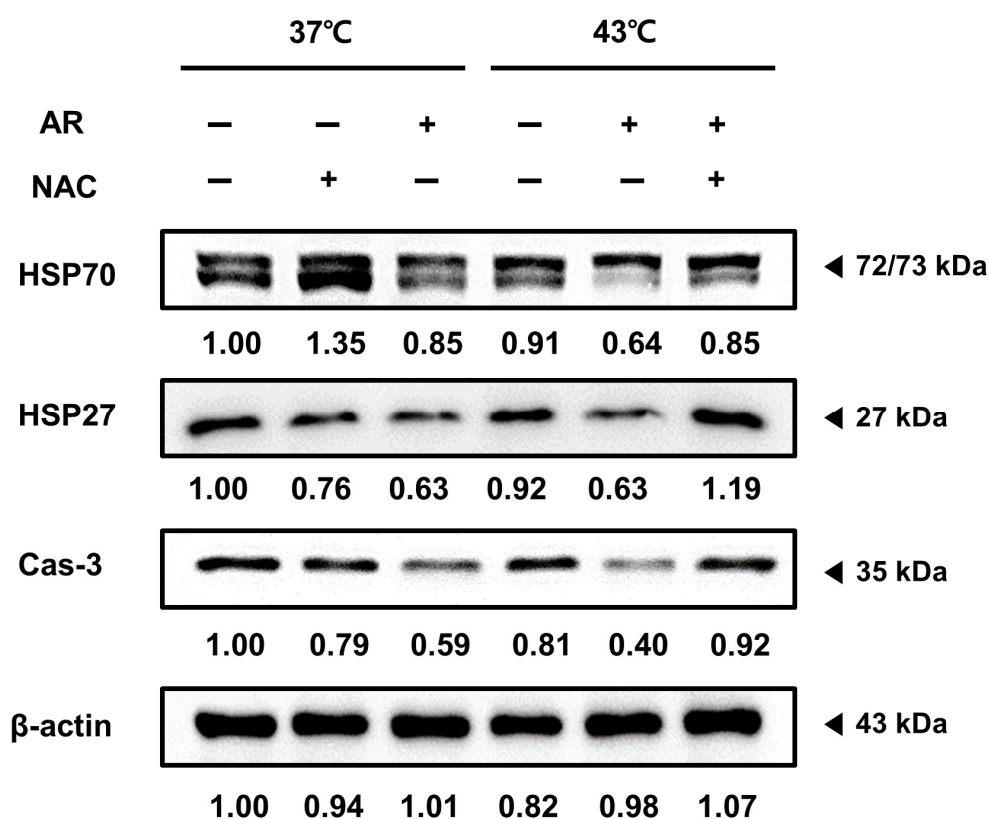


Figure 5. Effect of co-treatment with AR and HT on the mitogen-activated protein kinase (MAPK) pathway, apoptotic markers, and ROS production in ROS-inhibited AGS cells. AGS cells were pre-treated

with N-acetylcysteine (NAC) (5 mM) for 1 h before being exposed to AR (0 or 20  $\mu\text{g}/\text{mL}$ ) with (at 43  $^{\circ}\text{C}$ ) or without (at 37  $^{\circ}\text{C}$ ) HT. (A) HSP27, HSP70, and HSP90 expression. (B) Western blot assays were used to measure the concentrations of phosphor (p)-Jun N-terminal kinase (JNK), JNK, p-p38, p38, p-extracellular signal-regulated kinase (ERK), and ERK. (C) Flow cytometry was used to investigate ROS generation. (D) Apoptosis profiling was carried out in the presence of NAC or AR (+) and absence of NAC or AR (-).

### 3.6. ROS Scavenging Inhibited the Apoptotic Effect of the Combined AR and HT Treatment and Recovered HSP Expression

Next, we investigated whether NAC pretreatment could reverse the suppressed expression of HSP70, HSP27, and caspase-3 induced by the AR and HT co-treatment, suggesting that the co-treatment effects depended on ROS generation. Figure 6 shows that NAC pretreatment reversed the changes in expression of HSP70, HSP27, and caspase-3 induced by the co-treatment, indicating that the co-treatment effects were dependent, at least partly, on ROS and HSP.



**Figure 6.** Effect of co-treatment in ROS-inhibited AGS cells reduced apoptosis and increased HSP expression. Expressions of the proteins HSP70, HSP27, and caspase-3 in the presence of NAC or AR (+) and absence of NAC or AR (-). AGS cells ( $0.3 \times 10^6$ ) were pre-treated with NAC (5 mM) for 1 h before being exposed to AR with (at 43  $^{\circ}\text{C}$ ) or without (at 37  $^{\circ}\text{C}$ ) HT.

## 4. Discussion

Our study sought to investigate the synergistic effects of AR and HT at 43  $^{\circ}\text{C}$  on inhibiting AGS cancer cell proliferation and promoting apoptosis. The herbal extract AR, which is known for its rich costunolide and dehydrocostus lactone content, has been associated with significant anti-cancer activities [48–50]. To our knowledge, this is the first research that explores the synergistic effects of AR and 43  $^{\circ}\text{C}$  HT on cancer cells.

In our study, costunolide and dehydrocostus lactone, the two primary components of AR, drew significant attention. Both compounds are known for their broad-spectrum biological activities such as anti-inflammatory, anti-microbial, anti-ulcer, and anti-cancer features [51–54]. Notably, the mechanisms underlying their anti-cancer effects include inducing ROS and promoting apoptosis, which reflects our current findings [55–57]. Therefore, these two compounds may be the critical drivers of the synergistic effects observed in our study.

Our results demonstrated that the combination of AR and 43 °C HT led to a significant decrease in the viability and proliferation of AGS cells, pointing to the effectiveness of the treatment against cancer. These findings were further substantiated by the observable alterations in cell morphology, reduced cell migration, and diminished colony formation. We observed an enhanced induction of apoptosis under the combined treatment of AR and 43 °C HT, as evidenced by the increased cleavage of caspase-3, a key factor in programmed cell death [58]. This trend was mirrored in the levels of caspase-8 and caspase-9, which decreased under the combined treatment. Interestingly, this dose-dependent response was unique to the combined treatment, highlighting the distinctive potency of this approach.

Furthermore, this co-treatment induced apoptosis and suppressed anti-apoptotic factors Bcl-2 and Bcl-xL [59]. This dual action likely intensifies the apoptotic effects in AGS cells. This study also sheds light on the downregulation of factors related to metastasis and angiogenesis, such as Cyclin D1, VEGF, and MMP-9, under combined treatment, emphasizing the potential therapeutic promise of this strategy for controlling cancer cell proliferation and metastasis [60–63]. Importantly, the combined application of AR and 43 °C HT was found to induce cell cycle arrest at the G2/M phase, a process closely associated with the provocation of apoptosis [64,65]. Our findings suggest that the occurrence of apoptosis was dose-dependent under the combined treatment, suggesting the potential for a precise therapeutic approach.

Our study also revealed the critical role of ROS in the apoptotic effects of the combined treatment. HSPs, which are often linked to cell survival under stress, were inhibited by the combined treatment, resulting in increased ROS levels, which subsequently induced apoptosis. Notably, costunolide and dehydrocostus lactone have been reported to promote the generation of ROS, thereby enhancing oxidative stress and driving cancer cells toward apoptosis [66,67]. Thus, our findings are consistent with these previous reports, indicating that the ROS-mediated mechanism could be one of the key pathways involved in the synergistic anti-cancer effects of the combined treatment. However, when ROS were scavenged using NAC, a reversal of the apoptotic effect and recovery of HSP expression were observed, emphasizing the essential role of ROS in the desired therapeutic effects and indicating the potential limitations of this therapy in cancer cells with strong ROS-scavenging abilities.

In conclusion, our study offers compelling evidence to support the synergistic anti-cancer potential of AR and HT at 43 °C on AGS cells, mainly through promoting intrinsic apoptosis, inhibiting cell proliferation, and inducing cell cycle arrest (Figure 7). In particular, the presence of compounds such as costunolide and dehydrocostus lactone, which are known for their anti-cancer activities and roles in promoting ROS, likely enhances the effectiveness of combined AR and HT treatment [68–70]. These findings suggest that with the beneficial effects of costunolide and dehydrocostus lactone, the combination of AR and HT could emerge as a promising therapeutic approach for cancer treatment. However, future research should aim to prove this potential anti-cancer effects of AR and HT co-treatment in clinical settings.

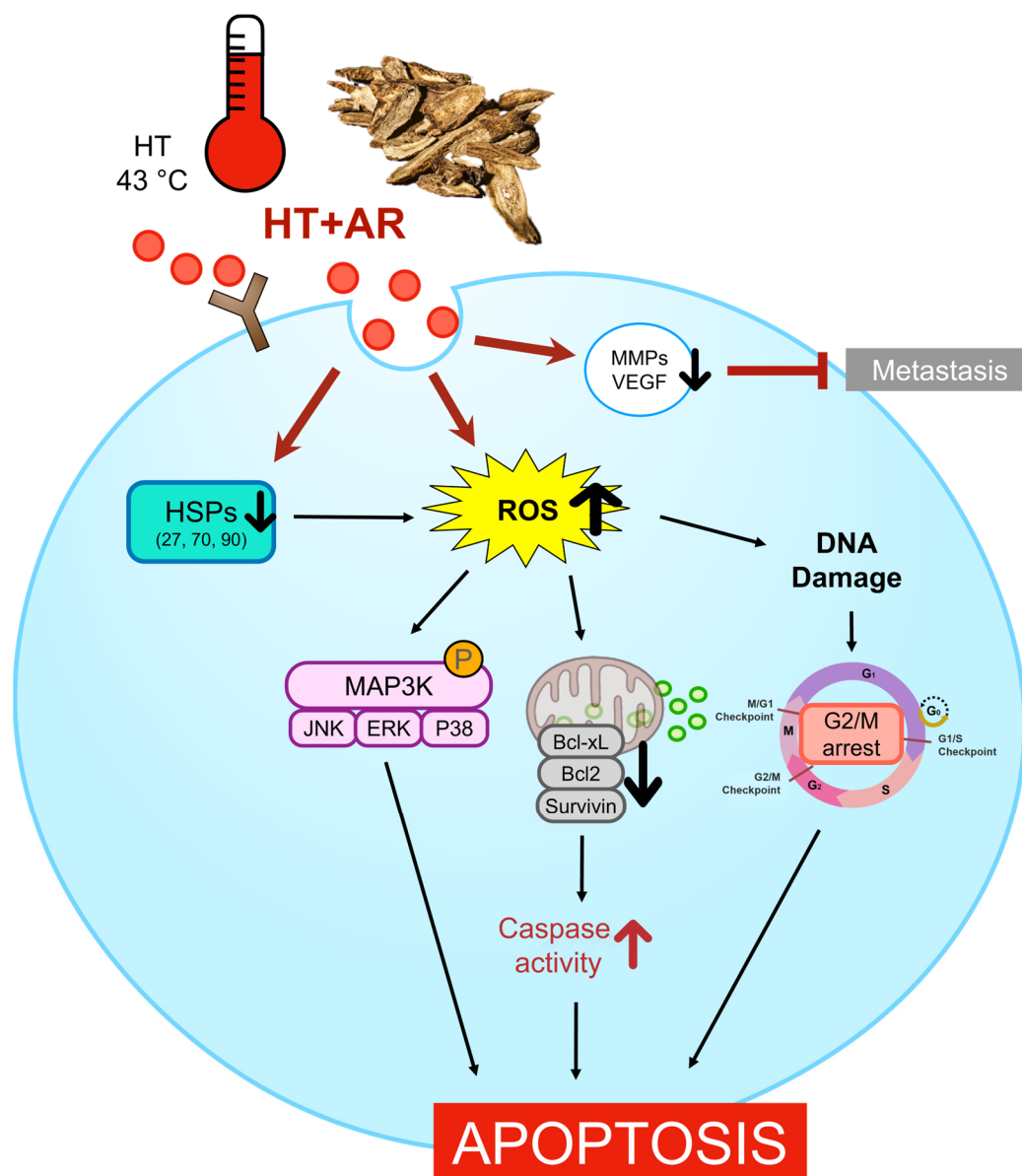


**Figure 7.** Schematic of the present study. Combination treatment with AR and 43 °C HT induces ROS-dependent intrinsic apoptosis in AGS cells. While HSF and HSP expressions are increased by HT, AR co-treatment suppresses the protective program in response to heat. AR and HT combination also induces cell cycle arrest, decreases expressions of MMPs and VEGF, and suppresses MAPK activation.

**Author Contributions:** Conceptualization, S.H.B.; methodology, J.-E.K., K.S.A., J.P. and S.H.B.; software, J.P. and S.H.B.; validation, C.R.A. and I.J.H.; formal analysis, C.R.A.; investigation, C.R.A. and I.J.H.; resources, J.P. and S.H.B.; data curation, C.R.A., J.P. and S.H.B.; writing—original draft preparation, C.R.A.; writing—review and editing, J.P. and S.H.B.; visualization, C.R.A., J.P. and S.H.B.; supervision, S.H.B.; project administration, J.P. and S.H.B.; funding acquisition, J.P. and S.H.B. All authors have read and agreed to the published version of the manuscript.

**Funding:** This work was supported by the Dongguk University Research Program of 2019, a grant from Kyung Hee University in 2022 (KHU-20220785), and a National Research Foundation of Korea (NRF) grant funded by the Korean Government (MSIP) (NRF-2020R1I1A3063625).

**Institutional Review Board Statement:** Not applicable.

**Informed Consent Statement:** Not applicable.

**Data Availability Statement:** The data presented in this study are available on request from the corresponding authors.

**Conflicts of Interest:** The authors declare no conflicts of interest.

## References

1. Hanahan, D.; Weinberg, R.A. Hallmarks of cancer: The next generation. *Cell* **2011**, *144*, 646–674. [[CrossRef](#)]
2. Siegel, R.L.; Miller, K.D.; Jemal, A. Cancer statistics, 2018. *CA Cancer J. Clin.* **2018**, *68*, 7–30. [[CrossRef](#)]
3. Bray, F.; Ferlay, J.; Soerjomataram, I.; Siegel, R.L.; Torre, L.A.; Jemal, A. Global cancer statistics 2018: GLOBOCAN estimates of incidence and mortality worldwide for 36 cancers in 185 countries. *CA Cancer J. Clin.* **2018**, *68*, 394–424. [[CrossRef](#)]
4. Mellman, I.; Coukos, G.; Dranoff, G. Cancer immunotherapy comes of age. *Nature* **2011**, *480*, 480–489. [[CrossRef](#)]
5. DeVita, V.T., Jr.; Chu, E. A History of cancer chemotherapy. *Cancer Res.* **2008**, *68*, 8643–8653. [[CrossRef](#)]
6. Formenti, S.C.; Demaria, S. Combining radiotherapy and cancer immunotherapy: A paradigm shift. *JNCI J. Natl. Cancer Inst.* **2013**, *105*, 256–265. [[CrossRef](#)]
7. Kwon, S.; Jung, S.; Baek, S.H. Combination Therapy of Radiation and Hyperthermia, Focusing on the Synergistic Anti-Cancer Effects and Research Trends. *Antioxidants* **2023**, *12*, 924. [[CrossRef](#)]
8. Marino, C.; Cividalli, A. Combined radiation and hyperthermia: Effects of the number of heat fractions and their interval on normal and tumour tissues. *Int. J. Hyperth.* **1992**, *8*, 771–781. [[CrossRef](#)]
9. Ahn, C.R.; Kim, H.I.; Kim, J.-E.; Ha, I.J.; Ahn, K.S.; Park, J.; Kim, Y.W.; Baek, S.H. Ponciri Fructus Immatarus Sensitizes the Apoptotic Effect of Hyperthermia Treatment in AGS Gastric Cancer Cells through ROS-Dependent HSP Suppression. *Biomedicines* **2023**, *11*, 405. [[CrossRef](#)]
10. van der Zee, J. Heating the patient: A promising approach? *Ann. Oncol.* **2002**, *13*, 1173–1184. [[CrossRef](#)]
11. Yi, G.Y.; Kim, M.J.; Kim, H.I.; Park, J.; Baek, S.H. Hyperthermia Treatment as a Promising Anti-Cancer Strategy: Therapeutic Targets, Perspective Mechanisms and Synergistic Combinations in Experimental Approaches. *Antioxidants* **2022**, *11*, 625. [[CrossRef](#)]
12. Zhuang, K.; Xia, Q.; Zhang, S.; Maharajan, K.; Liu, K.; Zhang, Y. A comprehensive chemical and pharmacological review of three confusable Chinese herbal medicine-Aucklandiae radix, Vladimiriæ radix, and Inulæ radix. *Phytother. Res.* **2021**, *35*, 6655–6689. [[CrossRef](#)]
13. Feng, L.; A, L.; Li, H.; Mu, X.; Ta, N.; Bai, L.; Fu, M.; Chen, Y. Pharmacological Mechanism of *Aucklandiæ Radix* against Gastric Ulcer Based on Network Pharmacology and In Vivo Experiment. *Medicina* **2023**, *59*, 666. [[CrossRef](#)]
14. Song, S.; Zhou, J.; Li, Y.; Liu, J.; Li, J.; Shu, P. Network pharmacology and experimental verification based research into the effect and mechanism of *Aucklandiæ Ra-dix-Amomi Fructus* against gastric cancer. *Sci. Rep.* **2022**, *12*, 9401. [[CrossRef](#)]
15. Shum, K.; Chen, F.; Li, S.; Wang, J.; But, P.P.; Shaw, P. Authentication of *Radix Aucklandiæ* and its substitutes by GC-MS and hierarchical clustering analysis. *J. Sep. Sci.* **2007**, *30*, 3233–3239. [[CrossRef](#)]
16. Cai, X.; Yang, C.; Qin, G.; Zhang, M.; Bi, Y.; Qiu, X.; Lu, L.; Chen, H. Antimicrobial Effects and Active Compounds of the Root of *Aucklandia Lappa Decne (Radix Aucklandiæ)*. *Front. Chem.* **2022**, *10*, 872480. [[CrossRef](#)]
17. Chen, Z.; Wei, C.; Yu, Z.; Yang, K.; Huang, Z.; Hu, H.; Wang, Z.-G. An effective method for preventing cholestatic liver injury of *Aucklandiæ Radix* and *Vladimiriæ Radix*: Inflammation suppression and regulate the expression of bile acid receptors. *J. Ethnopharmacol.* **2022**, *294*, 115330. [[CrossRef](#)]
18. Huang, Z.; Wei, C.; Yang, K.; Yu, Z.; Wang, Z.; Hu, H. *Aucklandiæ Radix* and *Vladimiriæ Radix*: A systematic review in ethnopharmacology, phytochemistry and pharmacology. *J. Ethnopharmacol.* **2021**, *280*, 114372. [[CrossRef](#)]
19. Chen, Y.; Miao, Z.; Sheng, X.; Li, X.; Ma, J.; Xu, X.; Li, H.; Kang, A. Sesquiterpene lactones-rich fraction from *Aucklandia lappa Decne.* alleviates dextran sulfate sodium induced ulcerative colitis through co-regulating MAPK and Nrf2/Hmox-1 signaling pathway. *J. Ethnopharmacol.* **2022**, *295*, 115401. [[CrossRef](#)]
20. Lin, X.; Peng, Z.; Su, C. Potential anti-cancer activities and mechanisms of costunolide and dehydrocostuslactone. *Int. J. Mol. Sci.* **2015**, *16*, 10888–10906. [[CrossRef](#)] [[PubMed](#)]
21. El-Far, A.H.; Godugu, K.; Salaheldin, T.A.; Darwish, N.H.E.; Saddiq, A.A.; Mousa, S.A. Nanonutraceuticals: Anti-Cancer Activity and Improved Safety of Chemotherapy by Costunolide and Its Nanoformulation against Colon and Breast Cancer. *Biomedicines* **2021**, *9*, 990. [[CrossRef](#)]
22. Choi, Y.-J.; Choi, Y.K.; Ko, S.-G.; Cheon, C.; Kim, T.Y. Investigation of Molecular Mechanisms Involved in Sensitivity to the Anti-Cancer Activity of Costunolide in Breast Cancer Cells. *Int. J. Mol. Sci.* **2023**, *24*, 4009. [[CrossRef](#)] [[PubMed](#)]
23. Lee, S.H.; Cho, Y.-C.; Lim, J.S. Costunolide, a Sesquiterpene Lactone, Suppresses Skin Cancer via Induction of Apoptosis and Blockage of Cell Proliferation. *Int. J. Mol. Sci.* **2021**, *22*, 2075. [[CrossRef](#)]
24. Li, Q.; Wang, Z.; Xie, Y.; Hu, H. Antitumor activity and mechanism of costunolide and dehydrocostus lactone: Two natural sesquiterpene lactones from the Asteraceae family. *Biomed. Pharmacother.* **2020**, *125*, 109955. [[CrossRef](#)] [[PubMed](#)]
25. Trachootham, D.; Alexandre, J.; Huang, P. Targeting cancer cells by ROS-mediated mechanisms: A radical therapeutic approach? *Nat. Rev. Drug Discov.* **2009**, *8*, 579–591. [[CrossRef](#)] [[PubMed](#)]
26. Wu, W.-S. The signaling mechanism of ROS in tumor progression. *Cancer Metastasis Rev.* **2006**, *25*, 695–705. [[CrossRef](#)] [[PubMed](#)]

27. He, M.; Wang, M.; Xu, T.; Zhang, M.; Dai, H.; Wang, C.; Ding, D.; Zhong, Z. Reactive oxygen species-powered cancer immunotherapy: Current status and challenges. *J. Control. Release* **2023**, *356*, 623–648. [[CrossRef](#)] [[PubMed](#)]
28. Zhang, C.; Lu, T.; Wang, G.-D.; Ma, C.; Zhou, Y.-F. Costunolide, an active sesquiterpene lactone, induced apoptosis via ROS-mediated ER stress and JNK pathway in human U2OS cells. *Biomed. Pharmacother.* **2016**, *80*, 253–259. [[CrossRef](#)] [[PubMed](#)]
29. Issels, R.D. Hyperthermia adds to chemotherapy. *Eur. J. Cancer* **2008**, *44*, 2546–2554. [[CrossRef](#)]
30. Reinhold, H.S.; Endrich, B. Tumour microcirculation as a target for hyperthermia. *Int. J. Hyperth.* **1986**, *2*, 111–137. [[CrossRef](#)]
31. Mallory, M.; Gogineni, E.; Jones, G.C.; Greer, L.; Simone, C.B. Therapeutic hyperthermia: The old, the new, and the upcoming. *Crit. Rev. Oncol. Hematol.* **2016**, *97*, 56–64. [[CrossRef](#)] [[PubMed](#)]
32. Song, C.W.; Shakil, A.; Osborn, J.L.; Iwata, K. Tumour oxygenation is increased by hyperthermia at mild temperatures. *Int. J. Hyperth.* **2009**, *25*, 91–95. [[CrossRef](#)]
33. Chatterjee, S.; Burns, T.F. Targeting Heat Shock Proteins in Cancer: A Promising Therapeutic Approach. *Int. J. Mol. Sci.* **2017**, *18*, 1978. [[CrossRef](#)] [[PubMed](#)]
34. Gümüş, M.; Koca, I.; Sert, Y.; Dişli, A.; Tunoğlu, E.N.Y.; Tutar, L.; Tutar, Y. Triad pyrazole–thiazole–coumarin heterocyclic core effectively inhibit HSP and drive cancer cells to apoptosis. *J. Biomol. Struct. Dyn.* **2023**, *41*, 14382–14397. [[CrossRef](#)]
35. Wu, J.; Liu, T.; Rios, Z.; Mei, Q.; Lin, X.; Cao, S. Heat Shock Proteins and Cancer. *Trends Pharmacol. Sci.* **2017**, *38*, 226–256. [[CrossRef](#)]
36. Ikwegbue, P.C.; Masamba, P.; Oyinloye, B.E.; Kappo, A.P. Roles of Heat Shock Proteins in Apoptosis, Oxidative Stress, Human Inflammatory Diseases, and Cancer. *Pharmaceuticals* **2018**, *11*, 2. [[CrossRef](#)] [[PubMed](#)]
37. Rosidi, B.; Priyatno, D.; Putra, T.P.; Yusuf, I. Metformin Induces a Caspase 3-Unrelated Apoptosis in Human Colorectal Cancer Cell Lines HCT116 and SW620. *Cancer Manag. Res.* **2023**, *15*, 475–485. [[CrossRef](#)]
38. Wu, Y.; Wang, D.; Wang, X.; Wang, Y.; Ren, F.; Chang, D.; Chang, Z.; Jia, B. Caspase 3 is Activated through caspase 8 instead of caspase 9 during H<sub>2</sub>O<sub>2</sub>-induced apoptosis in HeLa cells. *Cell. Physiol. Biochem.* **2011**, *27*, 539–546. [[CrossRef](#)]
39. Kale, J.; Osterlund, E.J.; Andrews, D.W. BCL-2 family proteins: Changing partners in the dance towards death. *Cell Death Differ.* **2018**, *25*, 65–80. [[CrossRef](#)]
40. Yang, F.; Wang, Y.-H.; Dong, S.-Y.; Chen, C.-Z.; Huang, D.-P. MLF1IP promotes cells proliferation and apoptosis by regulating CyclinD1 in breast cancer. *Int. J. Clin. Exp. Pathol.* **2017**, *10*, 11554–11562.
41. Ferrara, N. VEGF as a therapeutic target in cancer. *Oncology* **2005**, *69* (Suppl. S3), 11–16. [[CrossRef](#)] [[PubMed](#)]
42. John, A.; Tuszynski, G. The role of matrix metalloproteinases in tumor angiogenesis and tumor metastasis. *Pathol. Oncol. Res.* **2001**, *7*, 14–23. [[CrossRef](#)]
43. Shah, M.A.; Abuzar, S.M.; Ilyas, K.; Qadees, I.; Bilal, M.; Yousaf, R.; Kassim, R.M.T.; Rasul, A.; Saleem, U.; Alves, M.S.; et al. Ginsenosides in cancer: Targeting cell cycle arrest and apoptosis. *Chem. Interactions* **2023**, *382*, 110634. [[CrossRef](#)] [[PubMed](#)]
44. Shapiro, G.I.; Harper, J.W. Anticancer drug targets: Cell cycle and checkpoint control. *J. Clin. Investig.* **1999**, *104*, 1645–1653. [[CrossRef](#)] [[PubMed](#)]
45. Ling, Y.H.; El-Naggar, A.K.; Priebe, W.; Perez-Soler, R. Cell cycle-dependent cytotoxicity, G2/M phase arrest, and disruption of p34cdc2/cyclin B1 activity induced by dox-orubicin in synchronized P388 cells. *Mol. Pharmacol.* **1996**, *49*, 832–841.
46. Liang, H.-H.; Huang, C.-Y.; Chou, C.-W.; Makondi, P.T.; Huang, M.-T.; Wei, P.-L.; Chang, Y.-J. Heat shock protein 27 influences the anti-cancer effect of curcumin in colon cancer cells through ROS production and autophagy activation. *Life Sci.* **2018**, *209*, 43–51. [[CrossRef](#)] [[PubMed](#)]
47. Baek, S.H.; Kim, C.; Lee, J.H.; Nam, D.; Lee, J.; Lee, S.-G.; Chung, W.-S.; Jang, H.-J.; Kim, S.-H.; Ahn, K.S. Cinobufagin exerts anti-proliferative and pro-apoptotic effects through the modulation ROS-mediated MAPKs signaling pathway. *Immunopharmacol. Immunotoxicol.* **2015**, *37*, 265–273. [[CrossRef](#)] [[PubMed](#)]
48. Peng, Z.; Wang, Y.; Fan, J.; Lin, X.; Liu, C.; Xu, Y.; Ji, W.; Yan, C.; Su, C. Costunolide and dehydrocostuslactone combination treatment inhibit breast cancer by inducing cell cycle arrest and apoptosis through c-Myc/p53 and AKT/14-3-3 pathway. *Sci. Rep.* **2017**, *7*, 41254. [[CrossRef](#)]
49. Ahn; Choi, E.J.; Ahn, W.S. Antiproliferative effects of dehydrocostuslactone through cell cycle arrest and apoptosis in human ovarian cancer SK-OV-3 cells. *Int. J. Mol. Med.* **2009**, *23*, 211–216. [[CrossRef](#)]
50. Huang, H.; Yi, J.-K.; Lim, S.-G.; Park, S.; Zhang, H.; Kim, E.; Jang, S.; Lee, M.-H.; Liu, K.; Kim, K.-R.; et al. Costunolide Induces Apoptosis via the Reactive Oxygen Species and Protein Kinase B Pathway in Oral Cancer Cells. *Int. J. Mol. Sci.* **2021**, *22*, 7509. [[CrossRef](#)]
51. Butturini, E.; Di Paola, R.; Suzuki, H.; Paterniti, I.; Ahmad, A.; Mariotto, S.; Cuzzocrea, S. Costunolide and Dehydrocostuslactone, two natural sesquiterpene lactones, ameliorate the inflammatory process associated to experimental pleurisy in mice. *Eur. J. Pharmacol.* **2014**, *730*, 107–115. [[CrossRef](#)] [[PubMed](#)]
52. Wei, M.; Li, J.; Qiu, J.; Yan, Y.; Wang, H.; Wu, Z.; Liu, Y.; Shen, X.; Su, C.; Guo, Q.; et al. Costunolide induces apoptosis and inhibits migration and invasion in H1299 lung cancer cells. *Oncol. Rep.* **2020**, *43*, 1986–1994. [[CrossRef](#)] [[PubMed](#)]
53. Hua, P.; Sun, M.; Zhang, G.; Zhang, Y.; Song, G.; Liu, Z.; Li, X.; Zhang, X.; Li, B. Costunolide Induces Apoptosis through Generation of ROS and Activation of P53 in Human Esophageal Cancer Eca-109 Cells. *J. Biochem. Mol. Toxicol.* **2016**, *30*, 462–469. [[CrossRef](#)] [[PubMed](#)]
54. Jin, B.; Chen, Y.; Wang, J.; Chen, Y.; Zhang, M.; Huang, J.; Wang, Y. Costunolide alleviates hyperglycaemia-induced diabetic cardiomyopathy via inhibiting inflammatory responses and oxidative stress. *J. Cell. Mol. Med.* **2023**, *27*, 831–845. [[CrossRef](#)]

55. Gorrini, C.; Harris, I.S.; Mak, T.W. Modulation of oxidative stress as an anticancer strategy. *Nat. Rev. Drug Discov.* **2013**, *12*, 931–947. [[CrossRef](#)] [[PubMed](#)]
56. Sahebkar, A.; Malhotra, K.; Malik, A.; Almalki, W.H.; Kesharwani, P. Reactive oxygen species and its manipulation strategies in cancer treatment. *Curr. Med. Chem.* **2023**. [[CrossRef](#)] [[PubMed](#)]
57. Ku, J.M.; Kim, M.J.; Choi, Y.-J.; Lee, S.Y.; Im, J.-Y.; Jo, Y.-K.; Yoon, S.; Kim, J.-H.; Cha, J.W.; Shin, Y.C.; et al. JI017 Induces Cell Autophagy and Apoptosis via Elevated Levels of Reactive Oxygen Species in Human Lung Cancer Cells. *Int. J. Mol. Sci.* **2023**, *24*, 7528. [[CrossRef](#)] [[PubMed](#)]
58. Porter, A.G.; Jänicke, R.U. Emerging roles of caspase-3 in apoptosis. *Cell Death Differ.* **1999**, *6*, 99–104. [[CrossRef](#)] [[PubMed](#)]
59. Vishnu, W.K.; Abeesh, P.; Guruvayoorappan, C. Pyrazole (1, 2-diazole) induce apoptosis in lymphoma cells by targeting BCL-2 and BCL-XL genes and mitigate murine solid tumour development by regulating cyclin-D1 and Ki-67 expression. *Toxicol. Appl. Pharmacol.* **2021**, *418*, 115491. [[CrossRef](#)]
60. Behelgard, M.F.; Shahvir, Z.G.; Asghari, S.M. Apoptosis induction in human lung and colon cancer cells via impeding VEGF signaling pathways. *Mol. Biol. Rep.* **2022**, *49*, 3637–3647. [[CrossRef](#)]
61. Hosseini, S.; Chamani, J.; Hadipanah, M.R.; Ebadpour, N.; Hojjati, A.S.; Mohammadzadeh, M.H.; Rahimi, H.R. Nano-curcumin's suppression of breast cancer cells (MCF7) through the inhibition of cyclinD1 expression. *Breast Cancer Targets Ther.* **2019**, *11*, 137–142. [[CrossRef](#)]
62. Choi, E.K.; Kim, H.D.; Park, E.J.; Song, S.Y.; Phan, T.T.; Nam, M.; Kim, M.; Kim, D.-U.; Hoe, K.-L. 8-Methoxypsoralen Induces Apoptosis by Upregulating p53 and Inhibits Metastasis by Downregulating MMP-2 and MMP-9 in Human Gastric Cancer Cells. *Biomol. Ther.* **2023**, *31*, 219–226. [[CrossRef](#)] [[PubMed](#)]
63. Mi, C.; Shi, H.; Ma, J.; Han, L.Z.; Lee, J.J.; Jin, X. Celastrol induces the apoptosis of breast cancer cells and inhibits their invasion via downregulation of MMP-9. *Oncol. Rep.* **2014**, *32*, 2527–2532. [[CrossRef](#)] [[PubMed](#)]
64. Ahn, C.R.; Park, J.; Kim, J.-E.; Ahn, K.S.; Kim, Y.W.; Jeong, M.; Kim, H.J.; Park, S.H.; Baek, S.H. Cinnamaldehyde and Hyperthermia Co-Treatment Synergistically Induces ROS-Mediated Apoptosis in ACHN Renal Cell Carcinoma Cells. *Biomedicines* **2020**, *8*, 357. [[CrossRef](#)] [[PubMed](#)]
65. Singhal, S.; Vachani, A.; Antin-Ozerkis, D.; Kaiser, L.R.; Albelda, S.M. Prognostic implications of cell cycle, apoptosis, and angiogenesis biomarkers in non-small cell lung cancer: A review. *Clin. Cancer Res.* **2005**, *11*, 3974–3986. [[CrossRef](#)] [[PubMed](#)]
66. Rasul, A.; Bao, R.; Malhi, M.; Zhao, B.; Tsuji, I.; Li, J.; Li, X. Induction of apoptosis by costunolide in bladder cancer cells is mediated through ROS generation and mitochondrial dysfunction. *Molecules* **2013**, *18*, 1418–1433. [[CrossRef](#)] [[PubMed](#)]
67. Wang, Z.; Zhao, X.; Gong, X. Costunolide induces lung adenocarcinoma cell line A549 cells apoptosis through ROS (reactive oxygen species)-mediated endoplasmic reticulum stress. *Cell Biol. Int.* **2016**, *40*, 289–297. [[CrossRef](#)] [[PubMed](#)]
68. Yang, Y.-I.; Kim, J.-H.; Lee, K.-T.; Choi, J.-H. Costunolide induces apoptosis in platinum-resistant human ovarian cancer cells by generating reactive oxygen species. *Gynecol. Oncol.* **2011**, *123*, 588–596. [[CrossRef](#)] [[PubMed](#)]
69. Hung, J.-Y.; Hsu, Y.-L.; Ni, W.-C.; Tsai, Y.-M.; Yang, C.-J.; Kuo, P.-L.; Huang, M.-S. Oxidative and endoplasmic reticulum stress signaling are involved in dehydrocostuslactone-mediated apoptosis in human non-small cell lung cancer cells. *Lung Cancer* **2010**, *68*, 355–365. [[CrossRef](#)]
70. Peng, Y.; Zhou, T.; Wang, S.; Bahetjan, Y.; Li, X.; Yang, X. Dehydrocostus lactone inhibits the proliferation of esophageal cancer cells in vivo and in vitro through ROS-mediated apoptosis and autophagy. *Food Chem. Toxicol.* **2022**, *170*, 113453. [[CrossRef](#)]

**Disclaimer/Publisher's Note:** The statements, opinions and data contained in all publications are solely those of the individual author(s) and contributor(s) and not of MDPI and/or the editor(s). MDPI and/or the editor(s) disclaim responsibility for any injury to people or property resulting from any ideas, methods, instructions or products referred to in the content.